Tip-sample capacitance in electrostatic force microscopy

by

Peter Reichel

Bachelor thesis in physics
submitted to the department of physics, mathematics and computer science
(FB 08)
at the Johannes Gutenberg-University Mainz
on October 11^{th}, 2021

1. Supervisor: Prof. Dr. Stefan Weber
2. Supervisor: Prof. Dr. Jure Demsar

JOHANNES GUTENBERG UNIVERSITÄT MAINZ

JG|U

Peter Reichel
Max Planck Institute für Polymerforschung
Ackermannweg 10
55128 Mainz
Institut für Physik
Staudingerweg 7
Johannes Gutenberg-Universität D-55099 Mainz
pereiche@students.uni-mainz.de

Declaration

I hereby declare that I have written the present thesis independently and without use of other than the indicated means. I also declare that to the best of my knowledge all passages taken from published and unpublished sources have been referenced.The paper has not been submitted for evaluation to any other examining authority nor has it been published in any form whatsoever.

Mainz, October 11^{th}, 2021

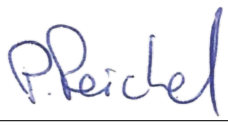

Peter Reichel

Erklärung

Hiermit versichere ich, dass ich die vorliegende Arbeit selbstständig und ohne Benutzung anderer als der angegebenen Hilfsmittel angefertigt habe. Die aus anderen Quellen oder indirekt übernommenen Daten und Konzepte sind unter Angabe der Quelle gekennzeichnet. Die Arbeit wurde bisher weder im In- noch Ausland in gleicher oder ähnlicher Form in einem Verfahren zur Erlangung eines akademischen Grades vorgelegt.

Mainz, den 11. Oktober 2021

Peter Reichel

Abstract (Englisch)

Tip-sample capacitance in electrostatic force microscopy is crucial for the research on dielectric properties of surfaces in nanometer scale. That is why we implement a new method of scanning capacitance microscopy. The aim of this method is to enhance existing methods by combining quantitative advantages and the reduction of stray capacitance by heterodyne frequency modulated Kelvin probe force microscopy with the capacitance resolution of nanoscale capacitance microscopy.
I demonstrate the capabilities of the method by displaying the change of the capacitance gradient on insulating polymer nanoparticles. Furthermore, I use a theoretical model probe to show that stray capacitance decreases for higher derivatives of the capacitance and the contribution of the tip apex dominates. With a force distance curve map that includes the capacitance signal of the method I show that the tip-sample capacitance decreases on the insulating polymer nanoparticles and that attofarad resolution can be achieved. Hence, the presented method shows promising potential for the investigation of dielectric properties of materials at the nanoscale. Furthermore, the method allows the use of two arbitrary electric excitation frequencies. Thus the dielectric response can be investigated as a function of frequency. Therefore, the method shows promising potential for an application in dielectric spectroscopy.

Abstract (Deutsch)

Die Spitzen-Proben-Kapazität in der elektrostatischen Kraftmikroskopie ist entscheidend für die Erforschung der dielektrischen Eigenschaften von Oberflächen im Nanometerbereich. Aus diesem Grund führen wir eine neue Methode der Rasterkraftmikroskopie ein. Ziel dieser Arbeit ist es, die bestehenden Methoden zu verbessern, indem die quantitativen Vorteile und die Verringerung der Streukapazität durch die heterodyne frequenzmodulierte Kelvinsonden-Kraftmikroskopie mit der Kapazitätsauflösung der Kapazitätsmikroskopie im Nanomaßstab kombiniert werden. Ich demonstriere die Möglichkeiten der Methode indem ich die Änderung des Kapazitätsgradienten auf isolierenden Polymer-Nanopartikeln darstelle. Darüber hinaus zeige ich anhand einer theoretischen Modellsonde, dass die Streukapazität für höhere Ableitungen der Kapazität abnimmt und der Beitrag des Spitzenscheitels dominiert. Mit einer Kraft-Abstands-Kurvenkarte, die das Kapazitätssignal der Methode einschließt, zeige ich, dass die Spitzen-Proben-Kapazität auf den isolierenden Polymer-Nanopartikeln abnimmt und, dass eine Attofarad- Auflösung erreicht werden kann. Die vorgestellte Methode zeigt daher ein vielversprechendes Potenzial für die Untersuchung der dielektrischen Eigenschaften von Materialien auf der Nanoskala. Außerdem erlaubt die Methode die Verwendung von zwei beliebigen elektrischen Anregungsfrequenzen. So können die dielektrischen Eigenschaften als Funktion der Frequenz untersucht werden. Daher zeigt die Methode ein vielversprechendes Potenzial für eine Anwendung in der dielektrischen Spektroskopie.

Contents

List of Figures

List of Tables

List of abbreviations

- AC - Alternating current
- AFM - Atomic force microscopy
- AM - Amplitude modulation
- CPD - Contact potential difference
- CV - Coefficient of variation
- DC - Direct current
- EFM - Electrostatic force microscopy
- DuFED - Dual frequency electrical drive
- FM - Frequency modulation
- InvOLS - Inverse optical lever sensitivity
- KPFM - Kelvin probe force microscopy
- PLL - Phase locked loop
- SCM - Scanning capacitance microscopy
- STM - Scanning tunneling microscopy
- vdW - van-der-Waals forces

1. Introduction

Atomic force microscopy (AFM) was invented by Binnig et al. [1] in 1986. Based on the force interaction between the surface of the sample and a nanometric tip attached to a flexible cantilever, they were able to achieve nanoscale and later atomic resolution [2] of the surface topography. This marks the beginning of one of the key technologies in the 21st century, nanotechnology. With the development of technological components that are getting smaller and smaller down to micrometer and even nanometer size, it is increasingly important to be able to measure dielectric properties at this scale [3].
Two different methods in AFM are used to measure electric properties of the surface in nanoscale. One is Kelvin probe force microscopy (KPFM) which adapts an AFM to measure the electric potential on surfaces [4]. The other is electrostatic force microscopy (EFM), where capacitive force between the tip and the sample is detected [5].
A promising technique in electrostatic force microscopy to obtain topography and capacitance simultaneously is scanning capacitance microscopy (SCM). The nanoscale capacitance is addressed using the probe as a nanometric electrode and the sample as a counter electrode. SCM was first introduced by Matey et al.[6] in 1985, where they used a high-frequency resonant capacitance sensor based on the frequency shift induced by the total tip–sample capacitance. This limited the measurements to materials with voltage dependent capacitance as found in semiconductors. Therefore a different method is needed to perform capacitance measurements on materials that do not show bias dependence e.g. dielectric films. An alternating current (ac) sensed method was introduced by Brezna et al. [7] to overcome these limitations, but it was not practical due to long data acquisition times. Fumagalli et al. [8] enhanced this method with a customized current amplifier and the lock-in integrated into the AFM electronics. Thus, they were able to reduce imaging time while remaining attofarad resolution. However, measurements were preformed in contact mode with a diamond coated cantilever tip. Hence, stray capacitance is non negligible.
Within the following bachelor thesis I will introduce a new scanning capacitance microscopy method called dual frequency electrical drive KPFM (DuFED-KPFM). The aim of this method is to combine the capacitance resolution of Fumagalli et al. [8] achieved in ac current sensing SCM with heterodyne frequency modulated (FM)-KPFM and its characteristics for the reduction of stray capacitance [9].
In DuFED-KPFM two electric drives with different frequencies are applied to the cantilever. A composition of these two electric frequencies causes a progression of change of the capacitance that is measured. In this process, local dielectric properties and topographic information can be measured simultaneously with high spatial resolution. In order to validate the measured results, a comparison with a numeric solution is drawn. In addition a quantitative interpretation of the appearing phenomena is provided.
Accordingly, the thesis is organized as follows. Chapter 2 covers the theoretical background. In chapter 3 the setup and the procedure of the experiment is presented. Furthermore the SCM method and its experimental implementation is introduced. Chapter 4 starts with a report of the capacitance images taken on a conductive silicon wafer

coated with insulating polymer nanoparticles. This is followed by a theoretical derivation of the tip sample capacitance with the aid of a model probe. For the last part of the analysis experimental values of the capacitance are determined with an evaluation of a force distance maps and compared to the theoretic values. Finally, in chapter 5 the results are discussed, a summary of the main conclusion is given and an outlook on further studies regarding the capacitance gradient in electrostatic force microscopy is provided.

2. Theoretical Background

2.1. AFM

Atomic force microscope (AFM) was invented by Binnig et al. [1] in 1986. It is a type of scanning probe microscope. Today it is widely used in physics, chemistry, biology, material science and engineering with different applications [10].
The principle of AFM is that a cantilever with a needle-like tip scans a surface in a grid pattern by sensing forces acting between the probe and the sample of interest. The cantilever behaves like a spring, for which Hook's law applies:

$$F = -k \cdot x, \tag{2.1}$$

where F is the force, k is the spring constant and x is the deflection of the cantilever. For distances far away from the surface, no forces act on the cantilever. As the distance decreases the cantilever enters the attractive regime, where van-der-Waals (vdW) forces act on the tip. At the same time the electrostatic force that has a longer range increases which is in contrast to the vdW forces of repulsive nature [11]. For very small distances the cantilever enters the repulsive regime, where Pauli repulsion is responsible for a repelling force on the tip which leads to bending of the cantilever. This deflection can be detected with a laser that is focused on the back of the cantilever by its reflection on a photodiode (Figure 2.1). Thus, the force can be obtained by the inverse optical lever sensitivity (InvOLS), which is the ratio between the the cantilevers z position, measured by the z-sensor and the deflection of the laser beam in volts that is measured by the photodiode [12].

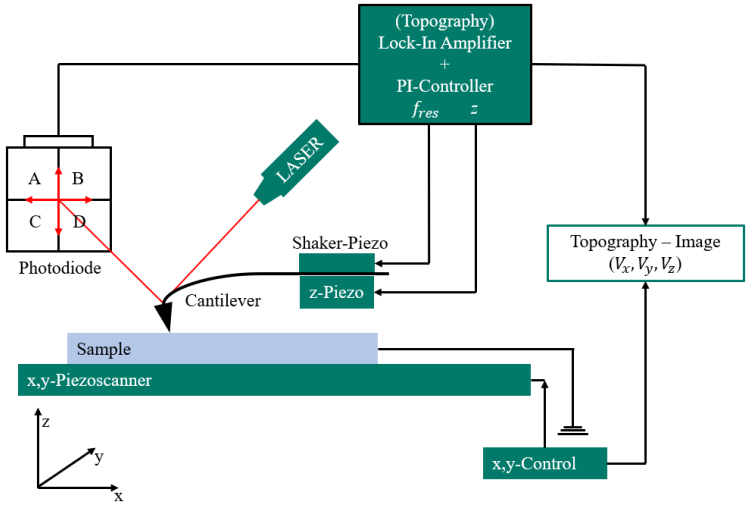

Figure 2.1.: Schematic setup of an AFM. The cantilever is excited by the shaker-piezo with its resonance frequency (f_{res}) and its position controlled by the z-piezo. It scans the sample in a grid-like pattern in x and y direction. The deflection is tracked by a laser which is reflected onto a position sensitive photodiode.

For the control of the cantilever in z-direction a *piezo* is used, while a x,y-piezoscanner is used to scan the sample in a grid-like pattern in x and y direction. A lock-in amplifier is used to detect the voltage of the measured signals. The measurement with an AFM can either be static, where the force is kept constant with a feedback circuit, or with a cantilever oscillating at its resonance frequency, where the amplitude and phase change drives the feedback circuit [1, 10]. This is how topography images with high resolution can be generated. AFMs can be used in many different applications such as topography imaging of the surface, scanning probe lithography or force spectroscopy [13]. However, I will only go into detail with the modes of operation that are used in the experiment.

2.2. KPFM

Kelvin probe force microscopy (KPFM) was introduced by M. Nonnenmacher et al. in 1991 [4] to characterize electrical surface properties in a nanometer scale. By applying an alternating voltage U_{AC} between a conducting tip and the sample, the system behaves like a capacitor with changing distance [14]. This enables the measurement of the contact potential difference (U_{CPD}) between the tip and the sample and produces oscillating electrical forces.
The contact potential difference describes the difference in Fermi levels between the surface and the tip (Figure 2.2). In equilibrium this corresponds to the work functions of the different materials

$$U_{CPD} = \frac{\Phi_{Tip} - \Phi_{Sample}}{-e}. \tag{2.2}$$

Here, Φ_{Tip} and Φ_{Sample} are the work functions of the materials respectively and e corresponds to the elemental charge. Therefore the work function of the sample can be determined if the work function of the cantilever is known [15].

To archive an equilibrium of the Fermi levels, an additional dc voltage U_{DC} has to be applied. This is shown in Figure 2.2.

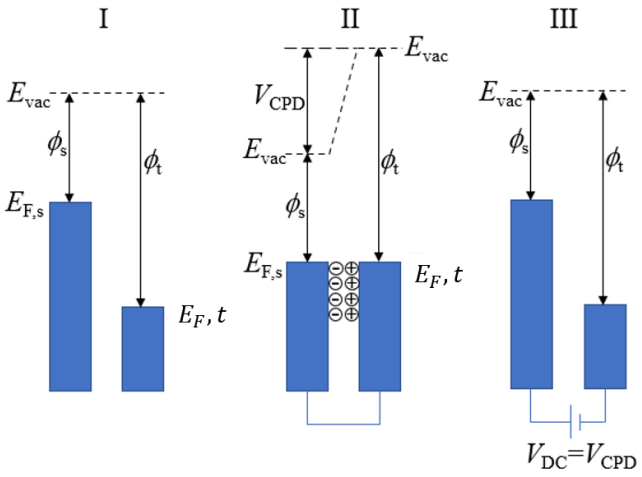

Figure 2.2.: Electronic energy levels between tip and sample for three different cases. In the first case tip and sample are separated and no voltage is applied. In the second case they are in electric contact and contact potential difference is building up. In the third case an additional voltage U_{DC} is applied which nullifies the contact potential difference U_{CPD} [15]

.

A schematic setup of a Kelvin force microscope is given in Figure 2.3. Additionally to a regular AFM an ac voltage is applied to the cantilever. This leads to the development of an electric field and therefore a change of the Fermi level. To align the Fermi levels again an additional dc voltage is required. This voltage minimizes the electrostatic force for $U_{DC} = U_{CPD}$. Thus, the contact potential difference can be measured. The response of the signal is detected with a lock-in amplifier.

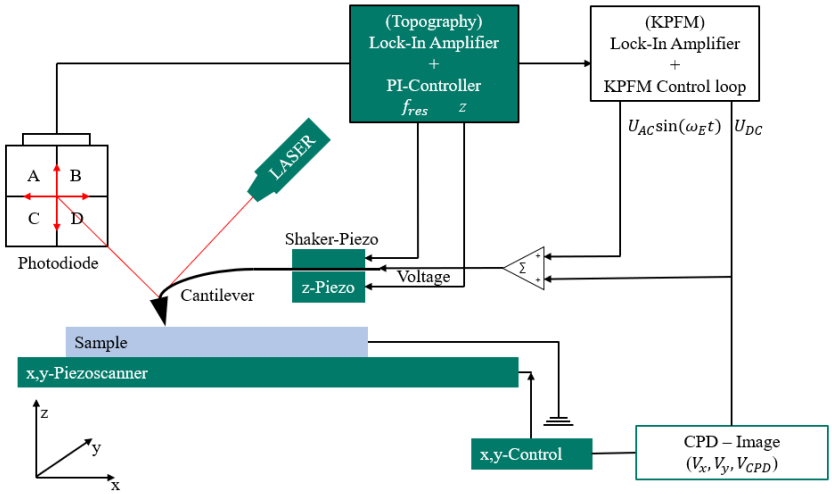

Figure 2.3.: Schematic setup of KPFM. An alternating voltage U_{AC} is applied between the tip and the sample and the response is tracked by a lock-in amplifier. This enables the measurement of the U_{CPD} on a nanometer scale.

By applying the external bias U_{DC}, the electrostatic forces between tip and the surface of the sample can be minimized. The electrostatic force F_{es} between the cantilever and the sample originates from the energy of a capacitor [16]. The following force is thus obtained via the gradient

$$F_{es} = \frac{1}{2}\frac{\partial C}{\partial z}(\Delta U)^2, \tag{2.3}$$

where $\frac{\partial C}{\partial z}$ is the capacitance gradient between the tip and the sample and ΔU is the difference between all the externally applied voltages and U_{CPD}. This gives $\Delta U = U_{ext} - U_{CPD}$, where U_{ext} is composed of $U_{ext} = U_{DC} + U_{AC}\sin(w_E t)$, where ω_E is the frequency of the applied ac voltage. The resulting electrostatic force can be divided into its spectral components

$$F_{stat.} = \frac{1}{2}\frac{\partial C}{\partial z}\left((U_{DC} - U_{CPD})^2 + \frac{U_{AC}^2}{2}\right) \tag{2.4}$$

$$F_{\omega_E} = \frac{\partial C}{\partial z}(U_{DC} - U_{CPD})U_{AC}\sin(\omega_E t) \tag{2.5}$$

$$F_{2\omega_E} = -\frac{1}{4}\frac{\partial C}{\partial z}U_{AC}^2\cos(2\omega_E t) \tag{2.6}$$

KPFM can be used in two acquisition modes: In amplitude modulation (AM) the response of the amplitude is tracked, whereas in frequency modulation (FM) variations of the cantilevers resonance frequency are tracked. According to Axt et al. [9], heterodyne-FM-KPFM is the best way to perform measurements of the quantitative surface potential.

2.2.1. FM-KPFM

In frequency modulated Kelvin probe force microscopy (FM-KPFM) variations of the cantilevers resonance frequency are tracked. These variations happen because of the

electrostatic force gradient.
When the tip of the cantilever approaches the sample, a shift in the angular resonance frequency occurs because of the forces acting on the cantilever. For oscillations with a small amplitude, this shift is approximately given by

$$\omega_0' \approx \sqrt{\frac{1}{m} \cdot \left(k - \frac{\partial F_{es}}{\partial z}\right)}, \tag{2.7}$$

where m is the mass, k is the spring constant of the undisturbed cantilever, and $\frac{\partial F_{es}}{\partial z}$ is the gradient of the force between tip and sample in z-direction [9].
This shift can be directly measured with a phase-locked loop (PLL), which is a controlled oscillator whose phase tracks that of an external signal [17]. The magnitude of the frequency modulation is proportional to the electrostatic force gradient and therefore proportional to the second derivative of the capacitance $\frac{\partial^2 C}{\partial z^2} = C''$ (Equation 2.3). Hence FM detection is sensitive to the electrostatic interaction between tip and surface of the sample and offers a high resolution [9].

The mechanical oscillation of the cantilever leads to an oscillation of the capacitance gradient with the same angular frequency ω_m. Thus, the capacitance gradient can be written as a Fourier series

$$C'(z) = \frac{a_0}{2} + \sum_{n=1}^{\infty} a_n \cos(n\omega_m t), \tag{2.8}$$

where a_0 and a_n are Fourier coefficients, ω_m is the mechanical oscillation of the cantilever and t is time. After inserting the capacitance gradient into the equation of the electrostatic force (2.3) and considering the Fourier coefficients up to n = 1, the following terms of the electrostatic force are obtained

$$F_{\omega_E} = \frac{\partial C}{\partial z}(U_{DC} - U_{CPD}) \cdot U_{AC} \sin(\omega_E t) \tag{2.9}$$

$$F_{2\omega_E} = -\frac{1}{4}\frac{\partial C}{\partial z} U_{AC}^2 \cos(2\omega_E t) \tag{2.10}$$

$$F_{\omega_m \pm \omega_E} = \frac{1}{2} A_m \frac{\partial^2 C}{\partial z^2}(U_{DC} - U_{CPD}) \cdot U_{AC} \left[sin\big((\omega_E - \omega_m)t\big) + \sin\big((\omega_E + \omega_m)t\big)\right]. \tag{2.11}$$

Here, A_m is the amplitude of the mechanical oscillation of the cantilever. It is noticeable, that Equation 2.9 and Equation 2.10 are identical to the AM-KPFM equations 2.5 and 2.6. However, Equation 2.11 shows that electrical signals are given on the sidebands $F_{\omega_m \pm \omega_E}$ with the mechanical oscillation ω_m. The sidebands are also dependent on the difference of $U_{DC} - U_{CPD}$ [**?**].
An enhancement to regular FM-KPFM is heterodyne-FM-KPFM [9]. It was introduced by Garrett et al. in 2016 [17]. By applying a mechanic frequency to the cantilever at its resonance frequency ω_0 and an electric frequency below its second eigenmode at $\omega_e = \omega_1 - \omega_0$, the sideband frequency gets shifted to the second eigenmode [17]. Thus, Equation 2.11 is the fundamental equation of heterodyne-FM-KPFM. A schematic representation of this is given in Figure 2.4. Heterodyne-Fm-KPFM leads to a superior sensitivity since the detection signal gets amplified by the resonance. Furthermore, the

electric excitation is separated from the detection, which excludes cross coupling and thus improves the signal to noise ratio [9].

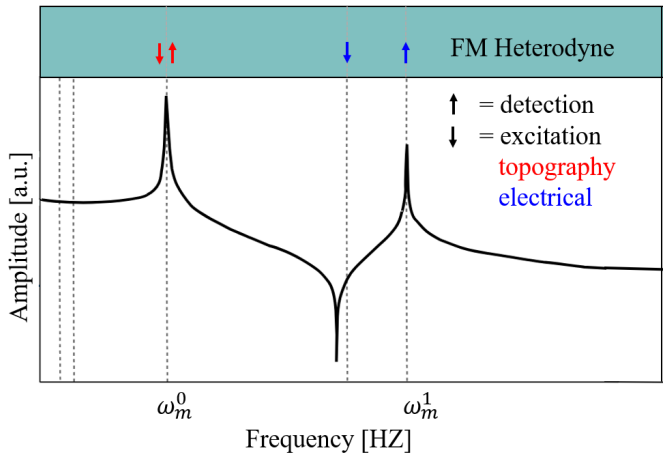

Figure 2.4.: Schematic diagram of the operating principle of heterodyne-FM-KPFM. At the resonance frequency ω_0 of the cantilever a mechanical frequency is applied to obtain topographical data. Furthermore an electric frequency is applied at $\omega_e = \omega_1 - \omega_0$ which shifts the signal that is detected to the second eigenmode of the cantilever [9].

The second derivative of the capacitance is proportional to the force gradient, which is more sensitive to local interactions between the tip of the cantilever and the sample surface than the force [18]. Hence, heterodyne-FM-KPFM offers a superior lateral and voltage resolution [19]. However, the force signal is usually stronger than the signal of the force gradient. Therefore high ac-voltages are required for heterodyne-FM-KPFM or FM-KPFM in general. These higher electrical drive amplitudes can cause a tip induced band bending at the surface [19].

2.3. Nanoscale capacitance microscopy

Scanning capacitance microscopy (SCM) was first introduced by Matey et al. [6] in 1985. It is used to identify dielectric properties of surfaces. The principle of SCM is that the probe is used as an electrode with the surface being the counter electrode. This enables the measurement of changes in the tip sample capacitance. Most common applications are the measurement of the depletion capacitance of semiconductors for carrier dopant profiling [20] or surface defect characterization [21]. The microscopes are typically equipped with a high-frequency resonant capacitance sensor which detects the frequency shift of the capacitor induced by the total tip–sample capacitance[22, 23]. The depletion capacitance under the tip apex is dependent on the applied voltage. That is why the signal is enhanced with an applied ac voltage modulation and the use of a lock-in detection technique[23].
Fumagalli et al. [8] developed a custom setup which is based on the ac current sensing and lock-in detection technique (Figure 2.5). This setup enables the nanoscale investigation of dielectric properties of the sample surface with non-voltage dependent capacitance.

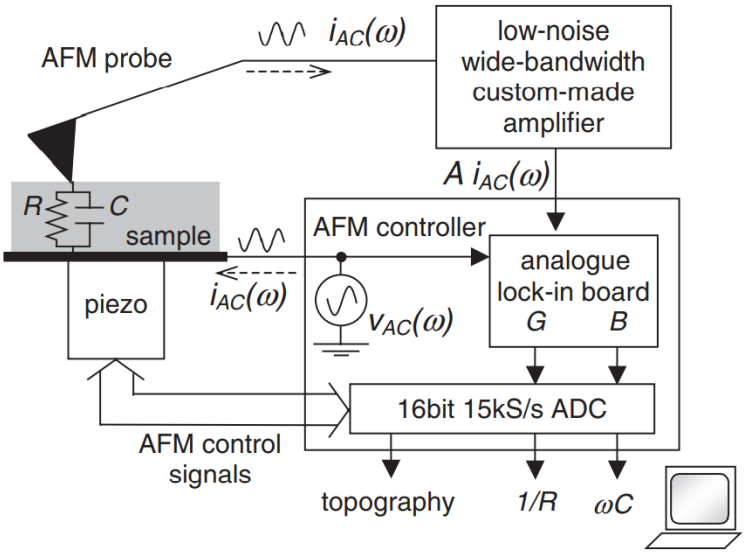

Figure 2.5.: Schematic setup of the nanoscale capacitance microscope. While scanning in contact with the surface, topography and capacitance can be obtained. The AFM probe is connected to a custom-made current-to-voltage amplifier, which is in turn connected to a lock-in board that is included in the AFM electronics [8]

By applying a low frequency ac voltage between the tip and the sample and using a low-noise wide-bandwidth custom-made amplifier, an electrostatic force can be detected with a lock-in amplifier. This electrostatic force translates into the first derivative of the local capacitance $\frac{\partial C}{\partial z}$ (compare Equation 2.3) and can be used to determine local dielectric properties. However, this method is very susceptible to stray capacitance. That is why only measurements on very thin dielectric films (~ 5 nm) can be performed. With the method we want to decrease the stray capacitance contributions to increase the applicability of the method.

2.4. Force-distance curve mapping

Force-distance curve mapping is usually used to measure nanomechanical properties such as Young's modulus, adhesion forces of the surface [24]. While maintaining the x,y-position, the AFM probe is ramped in z-direction and the vertical deflection of the cantilever is measured. The approach and retraction curves of the cantilever deflection versus the position of the z-piezo can be converted into force-distance curves that contain information of forces acting on the tip at a given location [24]. Among the forces acting on the tip is the electrostatic force [25]. Since the method measures the force gradient of the electrostatic interaction which translates to the second derivative of the capacitance, force-distance spectroscopy can be used to determine absolute capacitance values.
By taking force-distance curves on every pixel of an image, an entire force map can be generated and thus information about the capacitance of the entire map can be extracted. To obtain a force map, the operator has to set the position, the pixel size

of the image and up to which setpoint the deflection of the cantilever relative to the sample has to be measured.
Difficulties in force-distance curve mapping come from the amount of time that is required to record an entire image. A map of 300x300 pixels with a scan rate of 2 Hz takes up to 12 hours of measurement time. That is why thermal drift of the sample plays a big role in acquiring force maps. To solve this problem a lot of time is needed for the sample to adapt to the environmental conditions and to decrease the temperature gradient.

2.5. Capacitance in electrostatic force microscopy

When determining the capacitance in electrostatic force microscopy, the cantilever is used as a nanometric electrode with the sample being its counter electrode [26]. This assumption includes local capacitance contributions of the tip apex of the cantilever. However the assumption also includes non local capacitance contributions associated with the macroscopic cantilever, the mesoscopic tip cone and the chip holder [18].

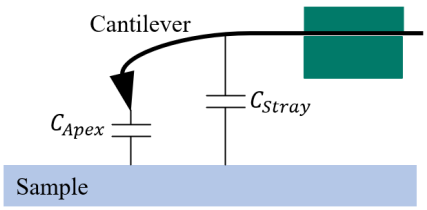

Figure 2.6.: Schematic illustration of stray capacitance. Between the tip-apex and the sample are local capacitance contributions that are deliberately measured, while the mesoscopic tip cone and the macroscopic cantilever contribute to interfering stray capacitance.

The problem in quantifying the electrostatic interaction is the complexity of the setup. That is why Colchero et al. [18] proposed a model system with three elemental building blocks: the tip apex, the tip cone and the cantilever. Assuming a model with the tip as a truncated cone with a spherical tip apex and the cantilever being a tilted rectangular plane capacitor [26, 27], yields the following equations for the force as a function of distance for the individual components of the probe:

$$F_{Lever}(z) = \frac{1}{2}\varepsilon_0 U^2 \frac{w \cdot l}{(z+h)^2} \frac{1}{(1+\frac{l}{z+h}\tan(\alpha))} \text{[27]} \tag{2.12}$$

$$F_{Cone}(z) = \frac{4\pi}{(\pi-\vartheta_{tip})^2}\varepsilon_0\varepsilon_r U^2 \left[ln\left(\frac{z-\frac{\delta}{2}+h}{z+\frac{\delta}{2}}\right) - \sin(\frac{\vartheta_{tip}}{2})\frac{h-\delta}{z-\frac{\delta}{2}+h} \cdot \frac{z-\frac{\delta}{2}}{z+\frac{\delta}{2}} \right] \text{[18]} \tag{2.13}$$

$$F_{apex}(z) = \pi\varepsilon_0\varepsilon_r r^2 U^2 \left[\frac{1-\sin(\frac{\vartheta_{tip}}{2})}{z(z+r(1-\sin(\frac{\vartheta_{tip}}{2})))} \right] \text{[26]}. \tag{2.14}$$

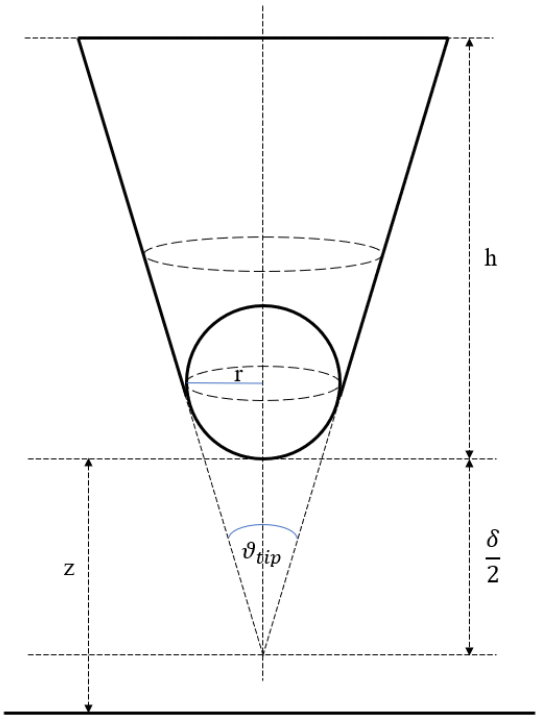

Figure 2.7.: Auxiliary sketch of the capacitance model of the truncated cone with spherical apex. Here h is the height of the tip, r is the radius of the sphere, ϑ_{tip} is the opening angle of the tip, δ is the truncated part of the cone and z is the distance between sample and tip apex.

Here, z is the distance between sample and tip apex, w is the width of the cantilever, l is the length of the cantilever and α is the angle in which the cantilever is tilted towards the surface. The cone has an opening angle of $\frac{\vartheta_{tip}}{2}$ and a height of h, whereas the height of the truncated part of the cone is $\delta = r/\tan^2(\frac{\vartheta_{tip}}{2})$. The spherical apex has a radius r as shown in Figure 2.7.
The capacitance of the model system can now be calculated by using Equation 2.3 and assuming that three components are connected in parallel.

3. Method and setup of the experiment

3.1. Method

For the measurement of the capacitance gradient I implement a new method. It is called "Dual frequency electrical drive KPFM" (DuFED-KPFM). The aim of this method is to enhance existing SCM methods [6, 8, 20, 23] by combining quantitative advantages and the reduction of stray capacitance by heterodyne-FM-KPFM [17] with the capacitance resolution of nanoscale capacitance microscopy [8].
For the method a mechanical drive at ω_m^0 at the fundamental eigenmode of the cantilever with amplitude A_m is used. Furthermore two electrical drives at frequency ω_1 and ω_2 with a voltage of U_1 and U_2 respectively are applied to the cantilever. In contrast to regular FM-KPFM this method is used without a feedback loop. This means no dc voltage U_{DC} is applied to the cantilever anymore. Thus, the electrostatic force is not compensated. This leads to

$$\Delta U = U_{CPD} + U_1 \sin(\omega_1 t) + U_2 \sin(\omega_2 t), \tag{3.1}$$

where ΔU corresponds to Equation 2.3. The open loop method accelerates data acquisition time of the measurement. Since the mechanical oscillation causes a periodic oscillation of the capacitance gradient, a Fourier expansion of $C'(t) = \frac{\partial C}{\partial z(t)}$ at z_0 results in

$$C'(z) = C'(z_0) + C''(z_0) A_m cos(\omega_m t) + \dots \ . \tag{3.2}$$

Equation 3.2 can now be substituted in Equation 2.3. Separating this equation into its spectral components yields the equations given in A.1.
The last term is given in 3.3.

$$\begin{aligned} F_{mix_2} = \frac{1}{2} C'' A_m U_1 U_2 \big(& cos[(\omega_m \pm \Delta\omega)t] \\ & + cos[(\omega_m + \omega_1 + \omega_2)t] - cos[(\omega_m - \omega_1 - \omega_2)t] \big) \end{aligned} \tag{3.3}$$

This is the fundamental equation of DuFED-KPFM. It contains the mechanical and the two electrical signals. The frequency modulation is proportional to the electrostatic force gradient and therefore to the second derivative of the capacitance. This means 3.3 yields a higher spatial resolution than F_{mix_1}.

In a high frequency regime the first cosine term of Equation 3.3 to probe the high frequency dielectric response can be used. It is given by

$$F_{mix2}^{HF} = \frac{1}{2} C'' A_m U_1 U_2 \big[cos((\omega_m \pm \Delta\omega)t) \big], \tag{3.4}$$

where $\Delta\omega = \omega_e = \omega_m^1 - \omega_m^0$ can be an arbitrary set of electrical drive frequencies that mix the response to the second eigenmode of the cantilever. Different harmonics

of multiples of ω_e can be used to obtain the given condition. This is inspired by FM-herterodyne-KPFM, where only a single electrical drive frequency is applied at $\omega_e = \omega_m^1 - \omega_m^0$.
The excitation and detection frequencies of the electrical and mechanical drives are schematically shown in Figure 3.1.

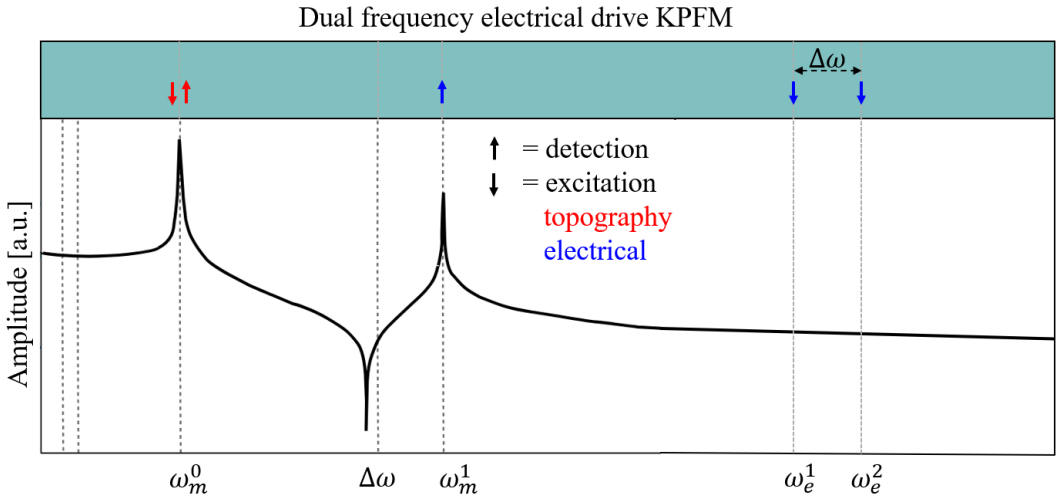

Figure 3.1.: Schematic illustration of the excitation and detection frequencies in dual frequency drive KPFM. The lower part shows the transfer function of the cantilever, where the amplitude is plotted vs the frequency. The upper part shows the excitation frequencies (↓) and the detection frequencies (↑) of the applied frequencies. The red arrow corresponds to topography- and the blue arrow to the electrical signal [9]

To implement the method a commercial AFM (*MFP-3D Infinity* from *Asylum Research*) is used for the measurement. As well as a lock-in amplifier (*HF2LI* from *Zürich Instruments*) for the electric excitation. The setup is shown in Figure 3.2. Thus, the respective ac voltages can be applied to the cantilever while measuring with the AFM. This enables the measurement of a capacitance image where the z-voltage is proportional to $\frac{\partial^2 C}{\partial z^2}$.

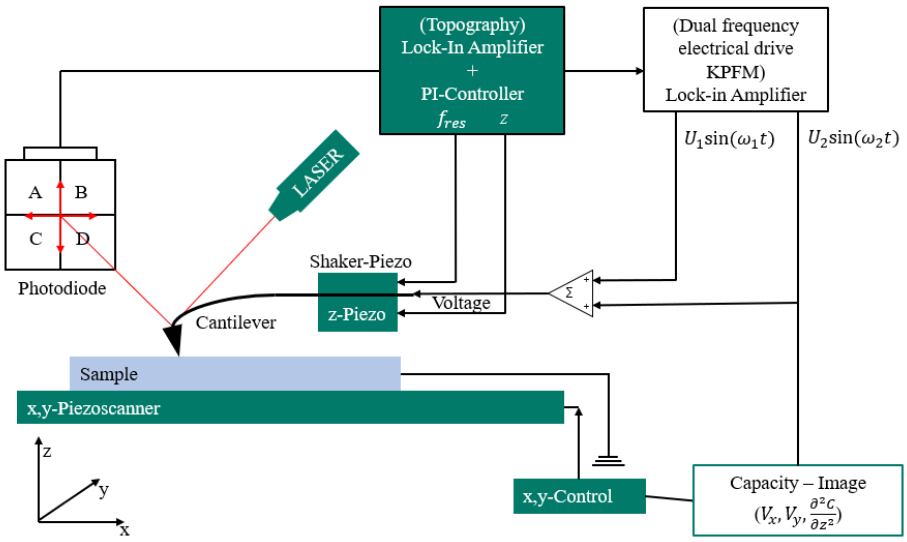

Figure 3.2.: Schematic setup of Dual frequency electrical drive KPFM. Additionally to a regular AFM, two different voltages are applied to the cantilever with different frequencies respectively.

3.2. Samples

All measurements were performed on silicon wafers, that were coated with Polystyrene(PS)-nanoparticles. The nanoparticles where ordered from *thermo scientific* as a latex microsphere suspension with an average diameter of 1.5 μm. The nanoparticles were dissolved in water with a weight concentration of 10% and a size distribution of $\leq 4\%$ for the coefficient of variation (CV). For my purposes I needed to reduce the concentration of the nanoparticles to get single particles on the surface of the silicon wafer. That is why I used *Methanol* to dilute the solution to a volume concentration of 0.001%.
The silicon wafers were prepared by cutting them into 2.5×2.5 cm pieces and using an airbrush to get rid of any dust particles that were left on the surface. After that the pieces were stored in an Argon plasma for 30 min at 290 W of power to clean the surface thoroughly.
The silicon wafers were then spin coated with the nanoparticle solution. For this, 80 μl of the solution were drobbed onto one wafer, which them was spin coated at 1000 rpm for 1 min.

3.3. Cantilever

For all experiments the cantilever model *SCM-PIT-V2* from Bruker [28] with a resonance frequency of typical $\approx 75\, kHz$ and a spring constant of $k \approx 3\, N/m$ is used. The cantilevers are usually $W \approx 35\, \mu m$ wide, $L = 225\, \mu m$ long and have a thickness of $T = 2.8\, \mu m$. They are made of 0.01 - 0.025 Ohm-cm Antimony (n) doped Silicon, whereas the front side is coated with conductive Platinum-Iridium (PtIr) and the back-

side is coated with reflective PtIr. The tip of the cantilever has a radius of $r = 25$ with a height of $h = 10 - 15\ \mu m$. Since the exact dimensions of the cantilever matter for calculations I performed later, the cantilevers were imaged via scanning electron microscope [29].

3.4. Data analysis

For the analysis of the measurement *Gwyddion 2.58*, *Igor Pro 6* and *Python 3.7.9* was used. For all images obtained in the measurement the color gradient *Gwyddion.net* was applied. For the height image set the minimal value of the image was set to zero and the data leveled by subtracting the mean level. If necessary the color leveling was adjusted to focus on the important parts of the image and eliminated scan line defects by aligning the rows by their median.
For all the creation of plots and fits, *Python*3.7.9 was used. Fit parameters and their respective errors were determined using $scipy.optimize.curve\_fit$. The code for the calculation of the capacitance in the force map is written with *Igor Pro 6* as well as the the fits that were used to determine the sample surface.

4. Analysis

4.1. Application of DuFED-KPFM

When recording images using the DuFED-KPFM method, several channels are recorded. This includes the images of the height, the amplitude and the phase of the oscillation of the cantilever, the voltage of the $\partial^2 C/\partial z^2$-Signal and the error of the signal. The cantilever scans the surface of the sample in a grid-like pattern. In this process information is being obtained during the outbound path (*Trace*) in x-direction and the return path (*Retrace*) in -x-direction of the cantilever (compare Figure A.1). To maintain comparability I use only *Retrace* images. Thereby all following images have a scan speed of 0.4 Hz and a resolution of 512 pixels × 512 pixels.
For all measurements I apply two voltages with 1 V on the 7^{th}, and 8^{th} harmonic of $\Delta\omega$ respectively.
Figure 3.2 shows an image of the sample taken with DuFED-KPFM. Here the left image shows the height information, whereas the right images displays the measured voltage signal that corresponds to the second derivative of the capacitance

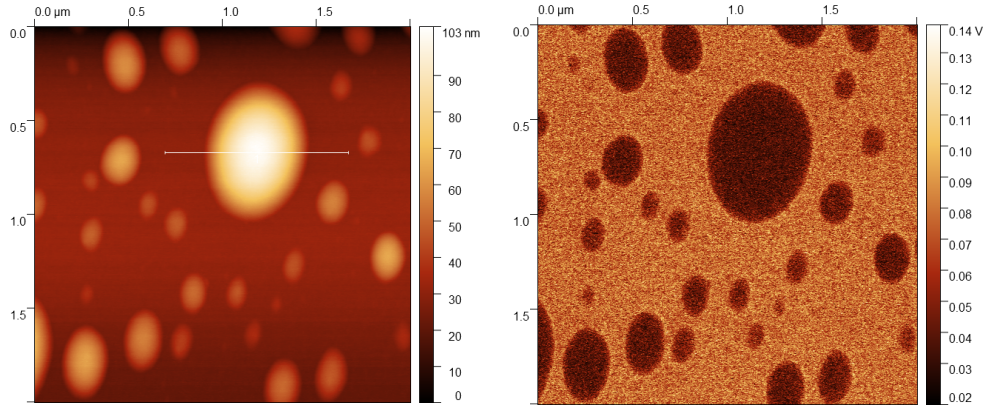

Figure 4.1.: Left: Height image, Right: Image of the voltage signal that corresponds to the second derivative of the capacitance of the polymer nanoparticles on a silicon surface. Along the included line the height and voltage signal profile is extracted.

It is evident that the right image in Figure 4.1 displays the particles that are displayed in the height-image on the left affirmative. This demonstrates the basic assumption that the method can display a changing signal on the particles. The first step in the investigation of the method to determine how the voltage signal, which corresponds to $\frac{\partial^2 C}{\partial z^2}$, behaves with increasing height.
For a regular plate capacitor, the capacitance is proportional to $C \sim \frac{1}{z}$ [16]. Considering this relation I would expect a similar dependency for the capacitance in the tip-sample system. Since a voltage is measured that corresponds to the second derivative of the

capacitance, the relation $C \sim \frac{1}{z}$ has to be derived twice to fit the measured signal. Thus, I expect a $\frac{\partial^2 C}{\partial z^2} \sim \frac{1}{z^3}$ dependency between the measured height and the voltage signal. To verify this assumption, I want to plot $\frac{\partial^2 C}{\partial z^2}$-signal versus the corresponding height. Hence, I extract the height information from the height-image across a nanoparticle. Additionally, I extract the voltage signal that corresponds to the second derivative of the capacitance for the same coordinates has for the height-image from the respective image. The resulting plot is given in Figure 4.2.

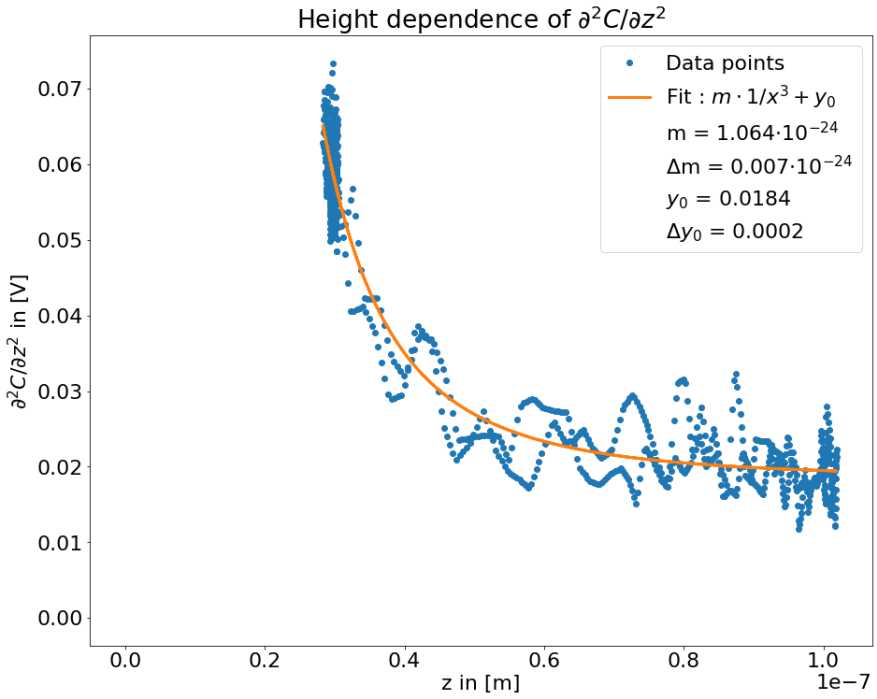

Figure 4.2.: Height profile of a nanoparticle plotted against the voltage signal of DuFED measurement. The blue dots represent the data points obtained with the measurement, while the orange line depicts a fit function of the form $f(x) = m/x^3 + y_0$.

It is noticeable that the fit I have chosen fits the data affirmative. However, an offset of $(y_0 = 18.4 \pm 0.2)mV$ needs to be included to adjust the function to the data points. This means that the signal converges to a minimum value on top of the particle and then remains constant.
Further examples are given in the appendix in A.4. Thus, a distinct signal difference between the conducting surface and the insulating nanoparticles can be measured. Moreover, it is shown that the signal decreases similarly with increasing size of the particle and converges to a constant value on the particles.
Therefore, I want to investigate the capacitance gradient further in the next chapters. For this purpose, I want to develop a theoretical model to show that the voltage is measured through the tip apex and that stray capacitance can be neglected. Furthermore, I want to quantify the measured results by evaluating a force map where the capacitance signal is also recorded as a function of distance and determine the resolution of the method.

4.2. Determination of theoretical values for the capacitance and its gradients

To determine theoretical values for the capacitance between the cantilever and the sample I use an adequate model that corresponds to the system. It is difficult to specify the exact values due to the complexity of the system. That is why Colchero et al. [18] proposed a simplified model that includes the tip apex, the cone and the cantilever. These three elemental building blocks of the tip-lever system interact with the sample as three capacitors that are connected in parallel. In nanoscale experiments the tip apex has the greatest influence in the measurement, whereas the cone and the cantilever are rather associated with stray capacitance. I assume, that the contribution of cone and cantilever is negligible for the second derivative of the capacitance. To verify this assumption, the contributions of the respective components are compared in the following.
The distance dependent force equations of the components are given in Equation 2.12 - Equation 2.14. To determine the capacitance of the components I use the basic equation for the electrostatic force of a capacitor

$$F_{es} = -\frac{1}{2}\frac{\partial C}{\partial z}U^2. \tag{4.1}$$

The capacitance can be obtained by integration of the equation for the electrostatic force as follows:

$$C(z) = -\int \frac{2F(z)}{U^2}dz \tag{4.2}$$

In the following I determine the capacitance of the respective components of the model probe.

4.2.1. Cantilever

The cantilever can be approximated by a tilted rectangular plane capacitor. In this case the electrostatic force is given by Equation 2.12. Integration yields

$$C_{lever}(z) = \varepsilon_0 \cdot \frac{w}{tan(\alpha)} \ln\left(1 + \frac{l \cdot tan(\alpha)}{h + z}\right), \tag{4.3}$$

where z is the distance between the sample and the tip apex and ε_0 is the dielectric constant of a vacuum. The dimensions of the lever are given by its width w, its length l and the height of the tip cone h. The lever is tilted by the angle α. Manufacturer specifications for the dimensions of the cantilever are considered (length = 225 μm, width = 35 μm). However, for the tip cone and apex SEM images were taken, to have more reliable results (Figure 4.3). Hence, the height of the tip cone is $14.63 \pm 0.5\mu m$. The error is given by 5% of the scale that was used to determine the height. I obtained the tilt angle of the cantilever by evaluating a picture of it taken in the cantilever holder from the AFM head A.5. The calculated capacitance is in the order of 2.2fF for the same distance as in the height profile of the nanoparticle (Figure 4.2). The corresponding plot is in the appendix in A.7.

4.2.2. Tip cone

The tip cone can be approximated by a truncated cone. The electrostatic force as a function of distance (z) between tip apex and sample is given by Equation 2.13. Integration of this equation to obtain the capacitance yields

$$C_{Cone}(z) = 2\frac{4\pi\varepsilon_0}{(\vartheta_{tip}-\pi)^2}\left[sin(\frac{\vartheta_{tip}}{2})(h\ln(2f_1)-\delta\ln(f_2))+f_1\ln\left(\frac{f_2}{2f_1}\right)+(\delta-h)\ln(f_2)\right], \tag{4.4}$$

where $f_1 = z - \frac{\delta}{2} + h$ and $f_2 = 2z + \delta$. By taking an SEM-image of the cantilever tip I was able to determine required quantities (Figure 4.3). Thus, the opening angle of the tip is $\vartheta = 19° + 24° = 43° \pm 1°$, the height of the tip is $h = 14.63 \pm 0.5\mu m$ and the truncated part of the cone is $\delta = r/\tan^2(\vartheta_t ip/2)$, where the radius is given by $r = 24.29 \pm 5nm$. The corresponding plot is in the appendix in Figure A.8

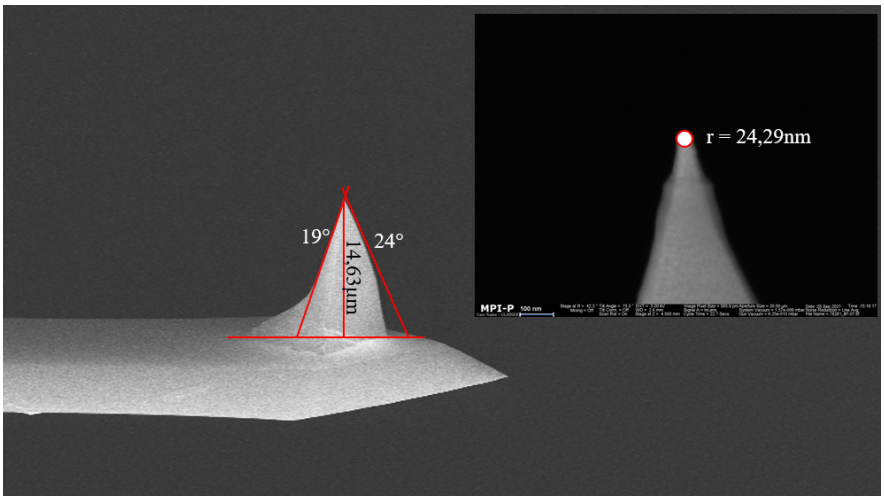

Figure 4.3.: Scanning electron microscopy images of the tip of the cantilever. Thus, the tip has a height of $14.63 \pm 0.5\mu m$, a front angle of $24° \pm 1°$, a back angle of $19° \pm 1°$, whereas the tip apex has a radius of $24.29 \pm 5nm$.

4.2.3. Apex

Finally, tip apex is approximated as a sphere over an infinite surface. The corresponding electrostatic force is given in Equation 2.14. Hence, the capacitance is given by

$$C_{apex}(z) = 2\pi\varepsilon_0\varepsilon_r r\ln\left(\frac{z+r(1-\sin(\frac{\vartheta_{tip}}{2}))}{z}\right), \tag{4.5}$$

where ε_r is the specific dielectric constant of the cantilever. Since the cantilever is made of silicon, it has a dielectric constant of $\varepsilon_r \approx 4$ [30]. The plot of the capacitance of the apex is given in the appendix in Figure A.7

4.2.4. Capacitance gradient of first and second order

To obtain the capacitance gradient of the first and second order I did an analytical derivation (A.2) as well as a numeric differentiation. Here only the numeric differentiation of the capacitance in the given range is considered. For this the differential

quotient for the onward and backward differentiation is used

$$f'(x) = \frac{f(x+h) - f(x-h)}{2h}) \tag{4.6}$$

with a step size of $1 \cdot 10^{-10}$ to have 1000 steps in the range of the DuFED measurement. Thus, I am able to obtain Figure 4.4 for the contribution of the respective components for the capacity gradient.

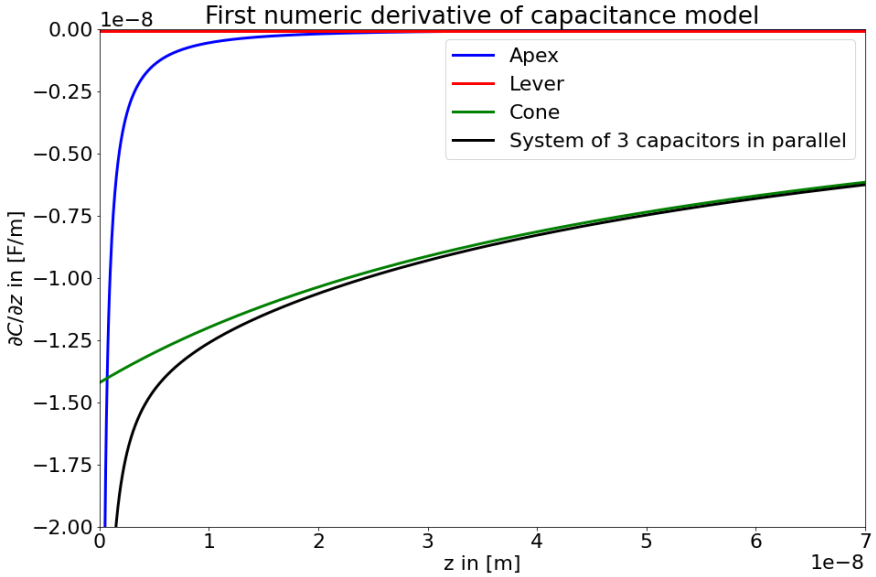

Figure 4.4.: Contribution to the capacitance gradient of the respective components. The blue line marks the apex, the green line the cone the red line the lever and the black line marks the entire system of the three components in parallel.

It is noticeable that the contribution of the lever is negligible. It is in the order of $81\frac{pF}{m}$ while the other two parts a several orders of magnitude higher with $\sim 10\frac{nF}{m}$.
For the capacitance gradient of the second order the central differential quotient of the second order is used

$$f''(x) = \frac{f(x+h) - 2f(x) + f(x-h)}{h^2} \tag{4.7}$$

with the same step size as for the first derivative. This gives us Figure 4.5 for the contributions of the respective components.

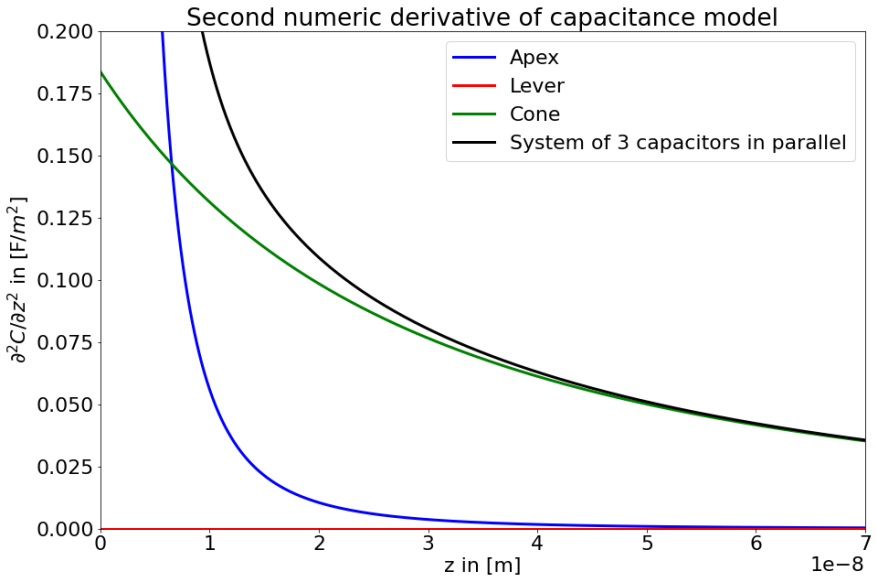

Figure 4.5.: Contributions of the respective components to the second numeric derivative of the capacitance. The blue line marks the apex, the green line the cone, the red line the lever and the black line marks the entire system of the three components in parallel. It is noticeable that the contribution of the tip surpasses the cone-contribution for distances smaller than $\approx 20nm$, while the contribution of the lever remains small.

From this can be concluded, that the contribution of the cantilever decreases for higher derivatives of the capacitance. Furthermore, the tip apex contribution exceeds the cone contribution for distances smaller than $\approx 20nm$.

4.3. Force map-Determination of the capacitance

The final step is the evaluation of a force map to determine the experimental capacitance resolution of DuFED-KPFM. For this a 150 × 150 pixel force map of 2 μm^2 surface area of the silicon wafer coated with polymer nanoparticles was take. The channels *Deflection*, *Amplitude*, *UserIn1*, *UserIn0* against time are recorded, where *UserIn1* corresponds to the voltage signal of $\partial^2 C/\partial z^2$ and *UserIn0* to the error signal. Thus, I was able to obtain the following force map.

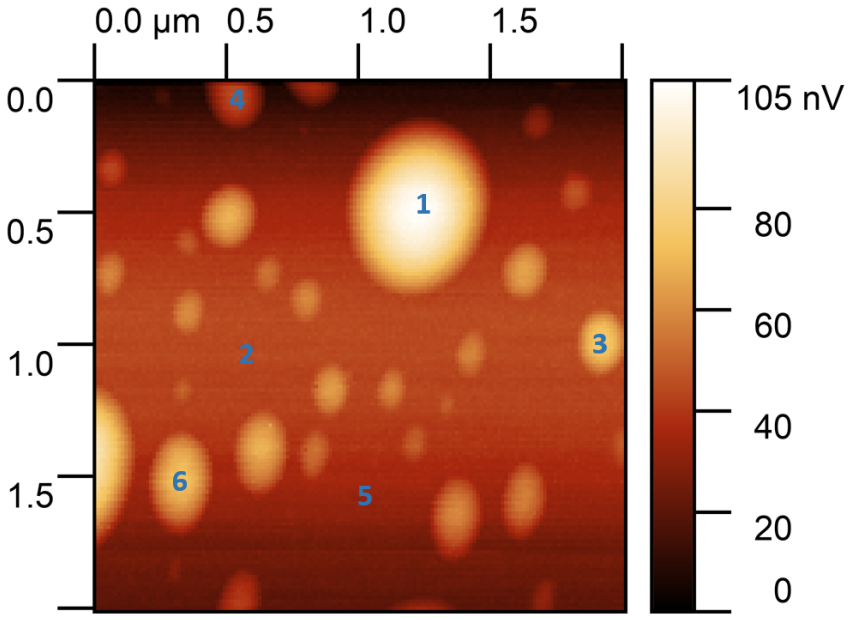

Figure 4.6.: Force map with 150 × 150 pixel covering a 2 μm^2 surface area of the silicon wafer coated with polymer nanoparticles. The blue numbers correspond to the locations, where I want to extract the measured capacitance.

To extract the measured capacitance from this force map the fundamental equation of DuFED (Equation 3.3) is used. Rearranging this equation to obtain the capacitance yields

$$\frac{\partial^2 C}{\partial z^2} = \frac{2F_{mix2}}{A_m U_1 U_2} \cdot \frac{1}{\cos((\omega_m \pm \Delta\omega)t) + \cos((\omega_m + \omega_1 + \omega_2)t) - \cos(\omega_m - \omega_1 - \omega_2)t]}. \tag{4.8}$$

One can assume, that the time that is required to obtain the capacitance approaches zero. Integrating $\partial^2 C/\partial z^2$ twice and using the assumption $\cos(\alpha) = 1; \alpha \to 0$ yields

$$C = \int \int_{z_{min}}^{z_{max}} \frac{2F_{mix2}}{A_m U_1 U_2} dz^2 \tag{4.9}$$

with

$$F_{mix2} = \frac{40}{100} k_0 \cdot S_{DuFED(\omega_e)} \cdot InvOLS. \tag{4.10}$$

here k_0 is the thermal spring constant, $S_{DuFED(\omega_e)}$ is the signal of the electric excitation and InvOLS is the inverse optical lever sensitivity. Since the signal at the second

eigenmode of the cantilever is measured, the thermal spring constant needs to be multiplied by 40 to obtain the thermal spring constant of the second eigenmode [31]. While measuring, the voltage is amplified by a factor of 100. Thus, the signal needs to be divided by 100 to obtain the true value.
The limits of the integration interval comes from the maximum deflection of the cantilever z_{max} and the point where it reaches the surface z_{min} of the sample. Thus, the capacitance is given by

$$C = \int\int_{z_{min}}^{z_{max}} \frac{\frac{2\cdot 40}{100} k_0 \cdot S_{DuFED(\omega_e)} \cdot InvOLS}{A_m U_1 U_2} dz^2 \tag{4.11}$$

To obtain the the point where the cantilever touches the surface, two linear fits on the respective force-distance curve are used. The first fit, approximates the trace when the cantilever is not in contact with the sample. The second fit approximates the trace when the cantilever is in contact with the sample. The intersection of these to fits is the real surface of the sample. An exemplary illustration of this procedure is given in Figure 4.7

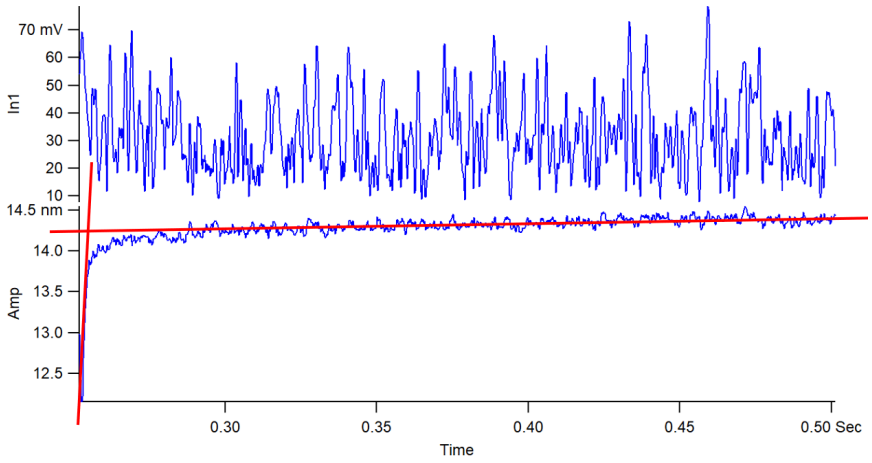

Figure 4.7.: Exemplary illustration of the determination of the real surface of the sample with the recorded amplitude over time during a force-distance curve map. The red lines represent the linear fits that were used.

This procedure was implemented in a code in Igor Pro 6.3 to evaluate the force map. The values for the InvOLS = 68.035 nm/V, and the spring constant calibrated by the thermal noise $k_0 = 2.94$ N/m are not reliable for our measurement as they were obtained with a different cantilever of the same type. Thus, the values for the obtained capacitance are not accurate, but they can be used as comparative values to support our assumption that the capacitance decreases on the insulating polymer particles. In Table 4.1 the values for the spots marked in Figure 4.6 are listed. However the fluctuations of the obtained capacitance were large. That is why several calculations for each spot are performed to calculate the mean value. The results are given in Table 4.1 respectively.

Spot in Figure 4.6	z_1 in $[\mu m]$	C in [aF]
1	2.6080 ± 0.0005	1.3150 ± 0.2051
2	2.6088 ± 0.0004	5.6697 ± 1.0932
3	2.6082 ± 0.0005	2.0303 ± 0.3219
4	2.6086 ± 0.0008	1.9977 ± 0.3176
5	2.6095 ± 0.0006	5.8229 ± 0.5532
6	2.6090 ± 0.0008	3.5483 ± 0.9612

Table 4.1.: The lower integration limit is received by finding the intersection of to linear fits (Figure 4.7). Then the capacitance values can be calculated by integrating the obtained force signal twice.

It is noticeable that the capacitance on polymer particles (spot: 1,3,4,6) is significantly lower than the capacitance on the silicon surface (spot: 2,5). This confirms our assumption that the capacitance decreases for the insulating spots.
However, this is not yet sufficient to obtain quantitative results for the capacitance. In further steps the entire force map needs to be evaluated and force maps with a higher resolution have to be obtained to investigate the fluctuations of the capacitance to determine what they are caused by. Furthermore, a more precise representation of the calculated surface is required since I was not able find a correlation between the capacitance and the calculated height. To solve this issue, more data is necessary.

5. Conclusion and Outlook

In conclusion the DuFED-KPFM method, which is a combination of *ac current sensing AFM* [8] and heterodyne-FM-KPFM [17] was introduced. I was able to record capacitance with $\sim$ 1 aF resolution. The dimension of the capacitance resolution is determined by noise of the system [23]. This is verified in Table 4.1, where the error of the measured capacitance is $\sim$ 1 aF.
Applying two electrical drives with the frequency being ω_e apart to the cantilever, which is mechanically oscillating at its resonance frequency enables the measurement of the second derivative of the capacity (Equation 3.3). Thus, I was able to display the change of the capacitance gradient on insulating polymer nanoparticles. Moreover, I could show the distance dependency of the capacitance gradient $\partial^2 C/\partial z^2 \sim \frac{1}{z^3}$. However, an offset in the voltage signal had to be included to fit the measured data affirmative. This offset is caused by the signal not disappearing over the particles..
A theoretical study of the cantilever was done by separating it into three components, being the tip apex, the cone and the lever. Thus, the capacitance contributions of the respective components could be determined. By a numerical derivation of the components I was able to determine the respective capacitance gradients and their contributions to the total capacitance. As a consequence I could show that the contribution of stray capacitance from the lever and the cone decreases for higher derivatives. For distances of less the 20nm between the tip and the sample the contribution of the apex prevails.
Force maps were recorded to determine the experimental capacitance resolution. By integrating the measured $\partial^2 C/\partial z^2$ signal twice over the z-range of the cantilever up to the true surface of the sample I was able to determine the capacitance between the tip-apex and the sample that is associated with the measurement. The values are not yet reliable for quantitative interpretation because the InvOLS and the thermal spring constant of a different cantilever were used for the calculation. However, our results show qualitatively accurate that the obtained capacitance decreases on the insulating nanoparticles and increases on the conductive surface. Furthermore, we can assume that the resolution is in the order of attofarad. Hence, the presented method shows promising potential for the investigation of dielectric properties of materials at the nanoscale. It is applicable for the measurement of thin films such as thin oxide films, biological membranes [4] or nanoparticles. Due to the low expected susceptibility to stray capacitance it would be interesting to see an investigation on thicker oxides ($\sim$ 50 nm) regarding its resolution. In further studies the dielectric constant of nanostructures can be determined. As a result label free detection of materials at the nanoscale is possible. Another application is dielectric spectroscopy [32]. Since the method enables the use of two arbitrary electric excitation frequencies, the frequency dependency of ϵ can be determined. Thus, the dielectric response according to the frequency can be investigated.

6. Bibliography

[1] Binnig, Quate, and Gerber.
Atomic force microscope.
Physical review letters, 56(9):930–933, 1986.

[2] Thomas R. Albrecht and Calvin F. Quate.
Atomic resolution with the atomic force microscope on conductors and nonconductors.
Journal of Vacuum Science & Technology A: Vacuum, Surfaces, and Films, 6(2):271–274, 1988.

[3] Eric Vogel.
Technology and metrology of new electronic materials and devices.
Nature nanotechnology, 2(1):25–32, 2007.

[4] M. Nonnenmacher, M. P. O'Boyle, and H. K. Wickramasinghe.
Kelvin probe force microscopy.
Applied Physics Letters, 58(25):2921–2923, 1991.

[5] G. Gramse, I. Casuso, J. Toset, L. Fumagalli, and G. Gomila.
Quantitative dielectric constant measurement of thin films by dc electrostatic force microscopy.
Nanotechnology, 20(39):395702, 2009.

[6] J. R. Matey and J. Blanc.
Scanning capacitance microscopy.
Journal of Applied Physics, 57(5):1437–1444, 1985.

[7] W. Brezna, M. Schramboeck, A. Lugstein, S. Harasek, H. Enichlmair, E. Bertagnolli, E. Gornik, and J. Smoliner.
Quantitative scanning capacitance spectroscopy.
Applied Physics Letters, 83(20):4253–4255, 2003.

[8] L. Fumagalli, G. Ferrari, M. Sampietro, I. Casuso, E. Martínez, J. Samitier, and G. Gomila.
Nanoscale capacitance imaging with attofarad resolution using ac current sensing atomic force microscopy.
Nanotechnology, 17(18):4581–4587, 2006.

[9] Amelie Axt, Ilka M. Hermes, Victor W. Bergmann, Niklas Tausendpfund, and Stefan A. L. Weber.
Know your full potential: Quantitative kelvin probe force microscopy on nanoscale electrical devices.
Beilstein journal of nanotechnology, 9:1809–1819, 2018.

[10] Bert Voigtländer, editor.
Scanning Probe Microscopy.
NanoScience and Technology. Springer Berlin Heidelberg, Berlin, Heidelberg, 2015.

[11] Hans-Jüurgen Butt.
Electrostatic interaction in atomic force microscopy.
Biophysical Journal, 60(4):777–785, 1991.

[12] Ryan Fuierer.
Basic operation procedures for the asylum research mfp-3dtmatomic force microscope, mfp-3d procedural operation 'manualette', 2006.

[13] Asylum Research - An Oxford Instruments Company.
Applications of atomic force microscopy (afm) - a guide, 09.10.2021.

[14] Kelvin.
V. contact electricity of metals.
The London, Edinburgh, and Dublin Philosophical Magazine and Journal of Science, 46(278):82–120, 1898.

[15] Wilhelm Melitz, Jian Shen, Andrew C. Kummel, and Sangyeob Lee.
Kelvin probe force microscopy and its application.
Surface Science Reports, 66(1):1–27, 2011.

[16] Dietmar Petrascheck and Franz Schwabl.
Elektrodynamik.
Springer Berlin Heidelberg, Berlin, Heidelberg, 2019.

[17] Joseph L. Garrett and Jeremy N. Munday.
Fast, high-resolution surface potential measurements in air with heterodyne kelvin probe force microscopy.
Nanotechnology, 27(24):245705, 2016.

[18] J. Colchero, A. Gil, and A. M. Baró.
Resolution enhancement and improved data interpretation in electrostatic force microscopy.
Physical Review B, 64(24), 2001.

[19] Th Glatzel, S. Sadewasser, and M.Ch Lux-Steiner.
Amplitude or frequency modulation-detection in kelvin probe force microscopy.
Applied Surface Science, 210(1-2):84–89, 2003.

[20] C. C. Williams.
Two-dimensional dopant profiling by scanning capacitance microscopy.
Annual Review of Materials Science, 29(1):471–504, 1999.

[21] K. V. Smith, E. T. Yu, J. M. Redwing, and K. S. Boutros.
Local electronic properties of algan/gan heterostructures probed by scanning capacitance microscopy.
Journal of Electronic Materials, 29(3):274–280, 2000.

[22] Y. Huang.
Capacitance–voltage measurement and modeling on a nanometer scale by scanning c–v microscopy.
Journal of Vacuum Science & Technology B: Microelectronics and Nanometer Structures, 12(1):369, 1994.

[23] David T. Lee, J. P. Pelz, and Bharat Bhushan.
Instrumentation for direct, low frequency scanning capacitance microscopy, and analysis of position dependent stray capacitance.
Review of Scientific Instruments, 73(10):3525–3533, 2002.

[24] Parksystems.
https://www.parksystems.com/park-spm-modes/95-force-measurement/244-force-distance-spectroscopy, 09.10.2021.

[25] Peter Eaton and Paul West.
Atomic Force Microscopy.
Oxford University Press, 2010.

[26] S. Hudlet, M. Saint Jean, C. Guthmann, and J. Berger.
Evaluation of the capacitive force between an atomic force microscopy tip and a metallic surface.
The European Physical Journal B, 2(1):5–10, 1998.

[27] B. M. Law and F. Rieutord.
Electrostatic forces in atomic force microscopy.
Physical Review B, 66(3), 2002.

[28] Bruker.
https://www.brukerafmprobes.com/p-3950-scm-pit-v2.aspx, 07.10.2021.

[29] The SEM images were obtained by Gunnar Glaser.

[30] Permittivität Wikipedia.
https://en.wikipedia.org/wiki/Relative_permittivity, 07.10.2021.

[31] Jose R. Lozano, Daniel Kiracofe, John Melcher, Ricardo Garcia, and Arvind Raman.
Calibration of higher eigenmode spring constants of atomic force microscope cantilevers.
Nanotechnology, 21(46):465502, 2010.

[32] Friedrich Kremer and Andreas Schönhals, editors.
Broadband Dielectric Spectroscopy.
Springer Berlin Heidelberg, Berlin, Heidelberg and s.l., 2003.

A. Appendix

A.1. Spectral components of electrostatic force in DuFED-KPFM

The spectral components of the electrostatic force in DuFED-KPFM are obtained by combining the equation for the electrostatic force (Equation 2.3) and the Fourier expansion of the capacitance gradient.

$$F_{DC} = \frac{1}{2}C'(U_{CPD} + \frac{U_1^2}{2} + \frac{U_2^2}{2}) \tag{A.1}$$

$$F_{\omega_m} = \frac{1}{2}C''A_m(U_{CPD} + \frac{U_1^2}{2} + \frac{U_2^2}{2})cos(\omega_m t) \tag{A.2}$$

$$F_{\omega_1,\omega_2} = C'U_{CPD}U_{1,2}sin(\omega_{1,2}t) \tag{A.3}$$

$$F_{2\omega_1,2\omega_2} = -\frac{1}{4}C'U_{1,2}cos(2\omega_{1,2}t) \tag{A.4}$$

$$F_{\omega_m \pm \omega_{1,2}} = \frac{1}{2}C''A_m U_{CPD}U_{1,2}sin[(\omega_m \pm \omega_{1,2})t] \tag{A.5}$$

$$F_{\omega_m \pm 2\omega_{1,2}} = -\frac{1}{8}C''A_m U_{1,2}cos[(\omega_m \pm 2\omega_{1,2})t] \tag{A.6}$$

$$F_{mix_1} = C'U_1U_2\big(sin[(\omega_1 - \omega_2)t] - cos[(\omega_1 + \omega_2)t]\big) \tag{A.7}$$

$$F_{mix_2} = \frac{1}{2}C''A_m U_1U_2\big(cos[(\omega_m \pm \Delta\omega)t] + cos[(\omega_m + \omega_1 + \omega_2)t] - cos[(\omega_m - \omega_1 - \omega_2)t]\big) \tag{A.8}$$

A.2. First and second analytic derivatives of the capacitance

First derivation of the capacitance of the model components respectively

$$\frac{\partial C}{\partial z}_{lever} = \varepsilon_0 \frac{w \cdot l}{(z+h)^2} \frac{1}{(1 + \frac{l}{z+h} tan(\alpha))} \tag{A.9}$$

$$\frac{\partial C}{\partial z}_{cone} = \frac{8\pi}{(\pi - \vartheta_{tip})^2} \varepsilon_0 \left[ln\left(\frac{z - \frac{\delta}{2} + h}{z + \frac{\delta}{2}} \right) - sin(\frac{\vartheta_{tip}}{2}) \frac{h - \delta}{z - \frac{\delta}{2} + h} \cdot \frac{z - \frac{\delta}{2}}{z + \frac{\delta}{2}} \right] \tag{A.10}$$

$$\frac{\partial C}{\partial z}_{apex} = 2\pi\varepsilon_0\varepsilon_r r^2 \left[\frac{1 - sin(\frac{\vartheta_{tip}}{2})}{z(z + r(1 - sin(\frac{\vartheta_{tip}}{2}))} \right] \tag{A.11}$$

Second derivation of the capacitance of the model components respectively

$$\frac{\partial^2 C}{\partial z^2}_{lever} = -\varepsilon_0 \frac{w \cdot l}{(z+h)^2} \frac{2(h+z) + l\tan(\alpha)}{(h + l\tan(\alpha) + z)^2} \tag{A.12}$$

$$\begin{aligned} \frac{\partial^2 C}{\partial z^2}_{cone} = \frac{8\pi}{(\pi - \vartheta_{tip})^2} \varepsilon_0 \Bigg[& -\frac{(h-\delta) sin(\frac{\vartheta_{tip}}{2})}{(\frac{\delta}{2} + z)(-\frac{\delta}{2} + h + z)} + \frac{(h-\delta) sin(\frac{\vartheta_{tip}}{2})(z - \frac{\delta}{2})}{(\frac{\delta}{2} + z)(-\frac{\delta}{2} + h + z)^2} \\ & + \frac{(h-\delta) sin(\frac{\vartheta_{tip}}{2})(z - \frac{\delta}{2})}{(\frac{\delta}{2} + z)^2(-\frac{\delta}{2} + h + z)} + \frac{(\frac{\delta}{2} + z)(\frac{1}{\frac{\delta}{2}+z} - \frac{-\frac{\delta}{2}+h+z}{(\frac{\delta}{2}+z)^2}}{-\frac{\delta}{2} + h + z} \Bigg] \end{aligned} \tag{A.13}$$

$$\frac{\partial^2 C}{\partial z^2}_{apex} = 2\pi\varepsilon_0\varepsilon_r r^2 \left[\frac{(2z + r(1 - sin(\frac{\vartheta_{tip}}{2})))(-1 + sin(\frac{\vartheta_{tip}}{2}))}{z^2(z + r(1 - sin(\frac{\vartheta_{tip}}{2})))^2} \right] \tag{A.14}$$

A.3. Channels obtained with the DuFED-measurement

On the left side are the *trace* images, whereas on the right side are the *retrace* images

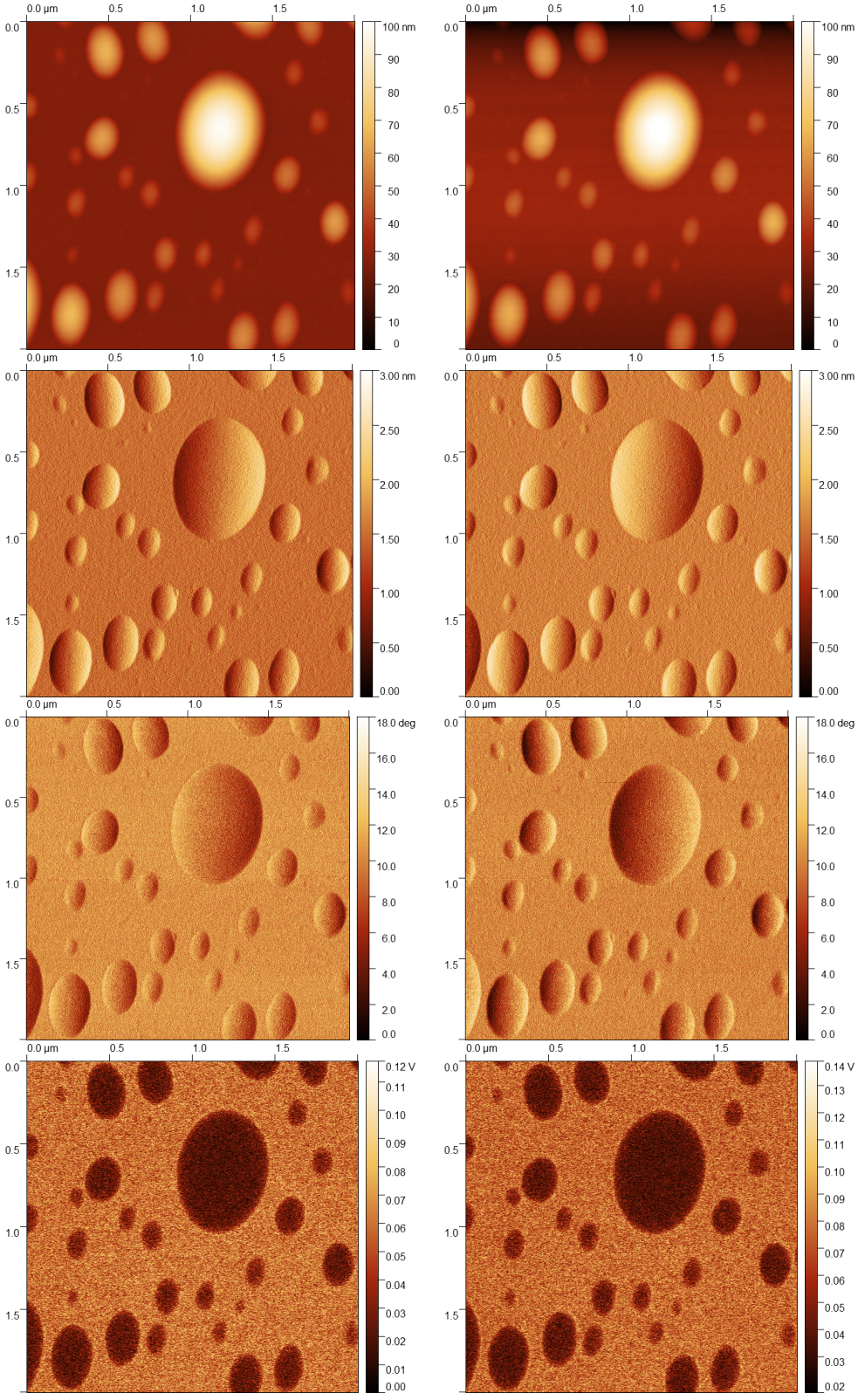
0.0 µm
0.5
1.0
1.5
100 nm
90
80
70
60
50
40
30
20
10
0
3.00 nm
2.50
2.00
1.50
1.00
0.50
0.00
18.0 deg
16.0
14.0
12.0
10.0
8.0
6.0
4.0
2.0
0.0
0.12 V
0.11
0.10
0.09
0.08
0.07
0.06
0.05
0.04
0.03
0.02
0.01
0.00
0.14 V
0.13

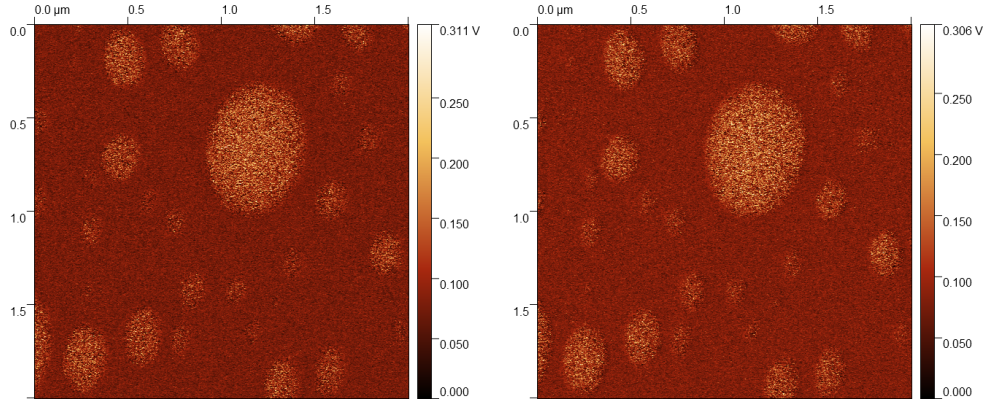

Figure A.1.: Left: *Trace*; Right: *retrace* images obtained with the DuFED-measurement. In the order: *Height*, *Amplitude*, *Phase*, *UserIn1*, *UserIn0*. Here *UserIn1* is the $\partial^2 C/\partial z^2$ signal, whereas *UserIn0* is the corresponging error signal.

A.4. Height dependence of the $\partial^2 C/\partial z^2$ signal

Profiles of the height and the $\partial^2 C/\partial z^2$ signal used in chapter 4:

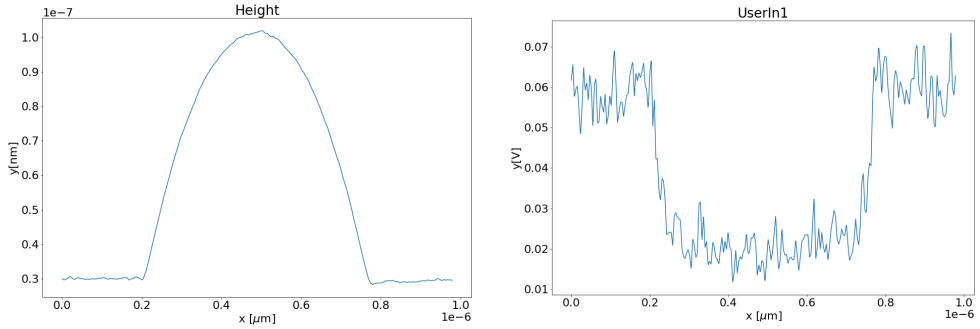

Figure A.2.: Left: Height image, Right: Image of $\partial^2 C/\partial z^2$-signal of the polymer nanoparticles on a silicon surface. Along the included line a the height and voltage signal profile is extracted.

To support the assumption given in chapter 4 this section provides more data.

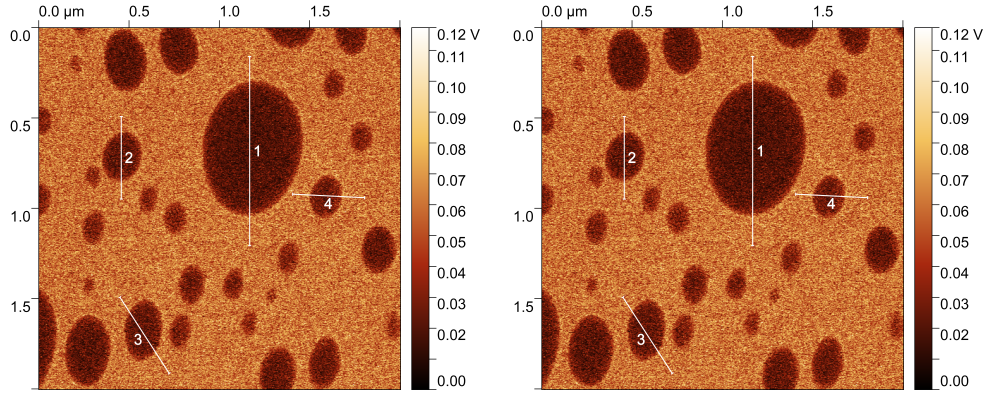

Figure A.3.: Left: Height image, Right: Image of $\partial^2 C/\partial z^2$-signal of the polymer nanoparticles on a silicon surface. Along the included line a the height and voltage signal profile is extracted.

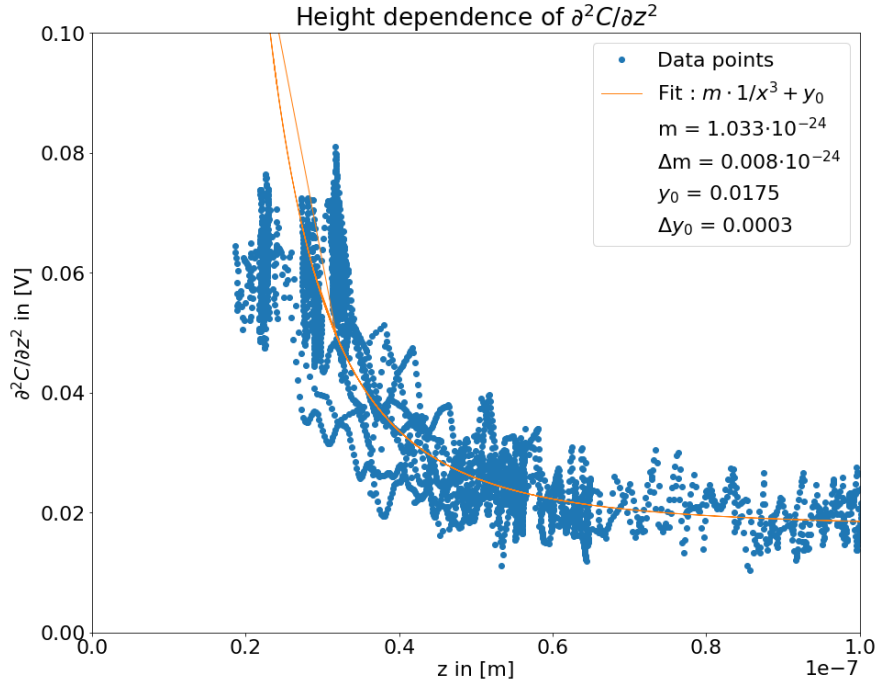

Figure A.4.: Supportive data of height profile of a nanoparticle plotted against the voltage signal of DuFED measurement. The blue dots represent the data points obtained with the measurement, while the orange line depicts a fit function of the form $f(x) = m/x^3 + y_0$.

A.5. Dimensions of Cantilever

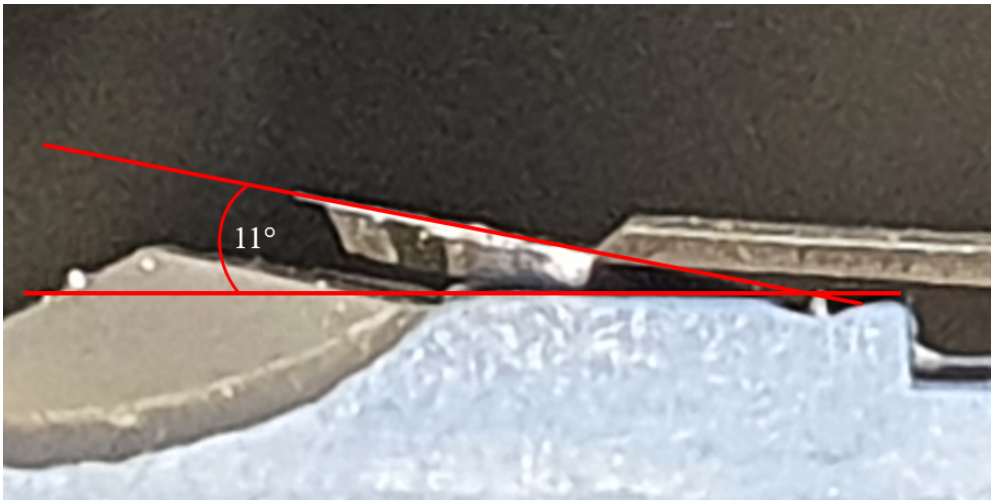

Figure A.5.: The angle of the cantilever inside the lever holder of the AFM is $\alpha = 11°$.

A.6. Capacitance model

In the following are the contributions of the respective components of the capacitance model

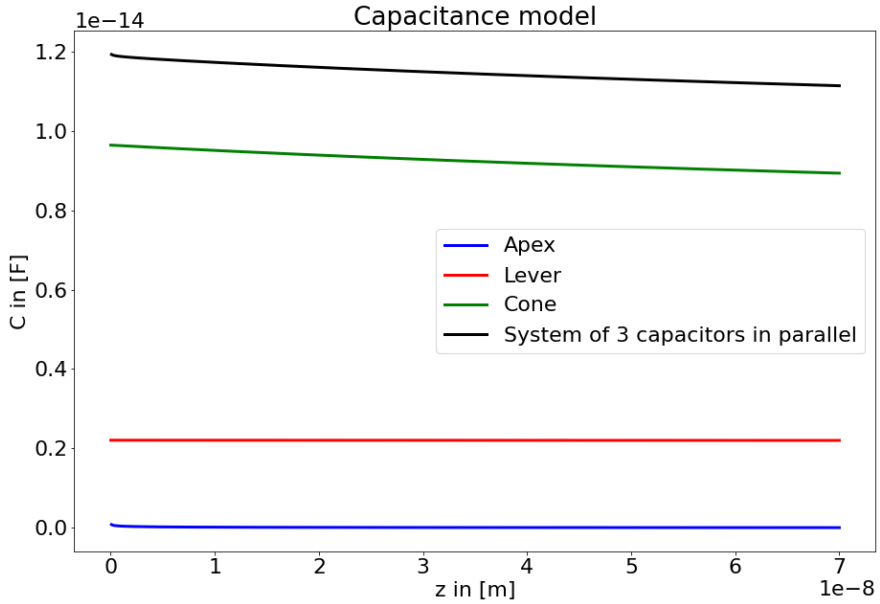

Figure A.6.: Capacitance model
Contribution to the capacitance of the respective components. The blue line marks the apex, the green line the cone, the red line the lever and the black line marks the entire system of the three components in parallel.

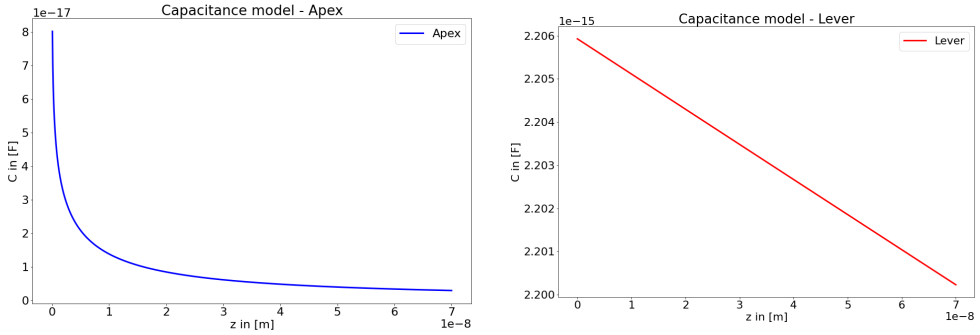

Figure A.7.: Left: Capacitance contribution of the apex.
Right: Capacitance contribution of the lever.

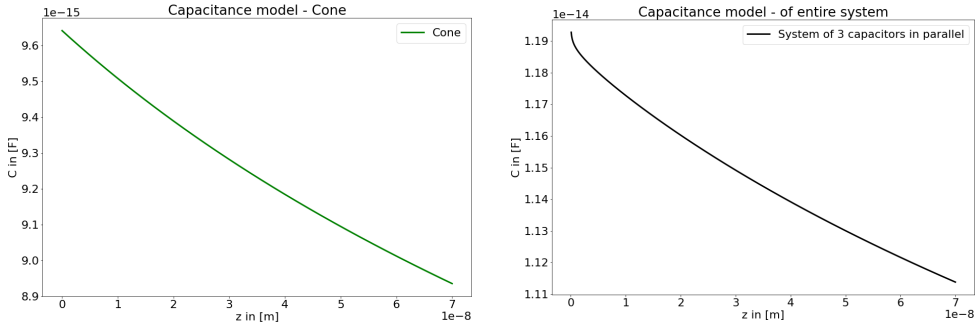

Figure A.8.: Left: Capacitance contribution of the cone.
Right: Capacitance contribution of the entire systems with the the components in connected in parallel.

B. Acknowledgment

At this point I would like to thank all those who have supported me in this work.

Special thanks go to Prof. Dr. Stefan Weber who welcomed me into his group and always was there for the excellent support and helpful discussions and suggestions.

Furthermore I want to say thank you to the Golden Boy M. Sc. Pascal Rohrbeck, who introduced me to the instruments and the research and always helped me when problems came up or I needed something to know.

I would like to thank all the group members of the Weber group for the warm welcome and the good work atmosphere during the time, as well as all the countless talks during lunch and coffee hours.